Multi-scale Computational Modeling for Concrete Damage Caused by Mixed Pore Pressures – Case of Coupled Alkali Silica Reaction and Freeze/thaw Cycles

Fuyuan Gong[1)], Yuya Takahashi[2)] and Koichi Maekawa[3)]

1) Fellow of Strategic Innovation Program, Department of Civil Engineering, The University of Tokyo
2) Assistant Professor, Department of Civil Engineering, The University of Tokyo
3) Professor, Department of Civil Engineering, The University of Tokyo

Abstract

As one kind of porous media, concrete suffers from some kinds of ambient impacts which may owe to the arising pore pressures. Freeze/thaw cycles (FTC) and alkali silica reaction (ASR) are such two typical impacts that may happen together, and cause mixed expansive pressure in micro-pores but finally result in macroscopic damage to concrete structures. In order to investigate the macro-mechanical behavior of concrete composites affected by the micro-events, a multi-scale computational model is developed based on the FEM computation program DuCOM-COM3 used in this study, the analysis system covers a wide range of scales from the hydration of cement paste to up-scaled mechanics of bulk structural concrete with cracks. The micro-physical events are computationally modeled by considering the coupling effect between ASR gel and condensed water in the mixed pressure and motion. The pressures and transport of pore substances are also linked with the concrete matrix deformation at macroscale through a poromechanical approach, and will affect each other, reciprocally. Once the crack happens in the nonlinear analysis, both the micro-events (water and gel motion) and the macro mechanics will be mutually interacted. Finally, different sequences of combined ASR and FTC are simulated. The multi-chemo mechanistic computation can reproduce the complex events in pore structures, and further the macro-damages. The results show that ASR can reduce the FTC expansion for non-air-entrained concrete but may increase the frost damage for air-entrained concrete. The simulation is examined to bring about observed phenomena.

Keywords: alkali-silica reaction, freeze-thaw cycles, strong coupling, multi-scale modeling, poro-mechanics

1. Introduction

Deterioration process of concrete is of high complexity since structural concrete usually suffers from coupled mechanistic and multiple ambient actions, such as high cycle fatigue loads, alkali silica reaction (ASR), freeze-thaw cycles (FTC), carbonation and steel corrosion. Considering the complexity of durability problems in terms of the coupling effects in chemical, physical and mechanical processes, a multi-scale modeling system is necessary to provide a strong linkage between each process and concrete material itself. The system should start from the hydration stage in nano-scale, and then be upgraded to the physics-chemical equilibrium in porous media, and finally lead to the structural performance (Maekawa *et al.*, 2003, Maekawa *et al.*, 2013). Based on this platform, several impacts have been modelled and simulated, such as the fatigue effect of condensed water under traffic loads (Maekawa and Fujiyama, 2013), the steel corrosion and crack opening caused by corrosion gels (Gebreyouhannes and Maekawa, 2016), as well as the ASR expansion and damage (Takahashi *et al.*, 2016). The above studies deal with one or dual impacts of weak coupling, which are rather ideal to predict the real complex deterioration process in real life. Thus, it is necessary to enhance the comprehensive modeling to take the strong interactive coupling of mechanistic and multiple environmental impacts into consideration. The first attempt of this study is the coupled FTC, ASR and condensed water motion accompanying crack kinematics.

The FTC and ASR damages take place together to concrete of many cases, and alternately in repeated winter and summer seasons. In addition, the deicing salt has been widely sprinkled on roads and bridge decks where the frost damage could happen, the remaining salt will also accelerate the ASR in the summer season (Kawamura *et al.*, 1994). The deterioration mechanisms by each single event have been widely investigated in the past decades. The frost damage is caused by the ice formation in pores and will be accumulated during numbers of FTC if additional water is supplied, finally will result in gradual degradation in material properties (Hasan *et al.*, 2004, Gong *et al.*, 2013). The expansive behavior of ASR and its modeling also have been well studied recently (Kawabata and Yamada, 2015, Costa *et al.*, 2014, Saouma, 2014, Saouma *et al.*, 2015, Multon *et al.*, 2009, Bažant and Steffens, 2000, Bangert *et al.*, 2004, Charpin and Ehrlacher, 2014, Takahashi *et al.*, 2016). For the major interactions between two impacts, previous experiments show that ASR gel can flow into entrained air voids, which can delay or reduce the ASR expansion (Jensen *et al.*, 1984) at early stage, but it will increase the risk of frost damage on the contrary. The ASR gel can also flow into existing crack gaps (Maraghechi *et al.*, 2012), which will affect the water permeation in the crack system. These events are so strongly and mutually coupled each other.

In this paper, the coupling between FTC and ASR will be modelled from the micro-structural level, by considering the ice formation and ASR gel intrusion into capillary pores, as well as the effect of entrained air. Then, based on the poro-mechanics, the mixed pore pressure and deformation of concrete skeleton will also be formulated by considering the multi-phase flows in pores. Finally, different sequences of combined FTC and ASR expansion will be simulated, and the results will be discussed in detail at different scales.

2. Multi-scale Modeling

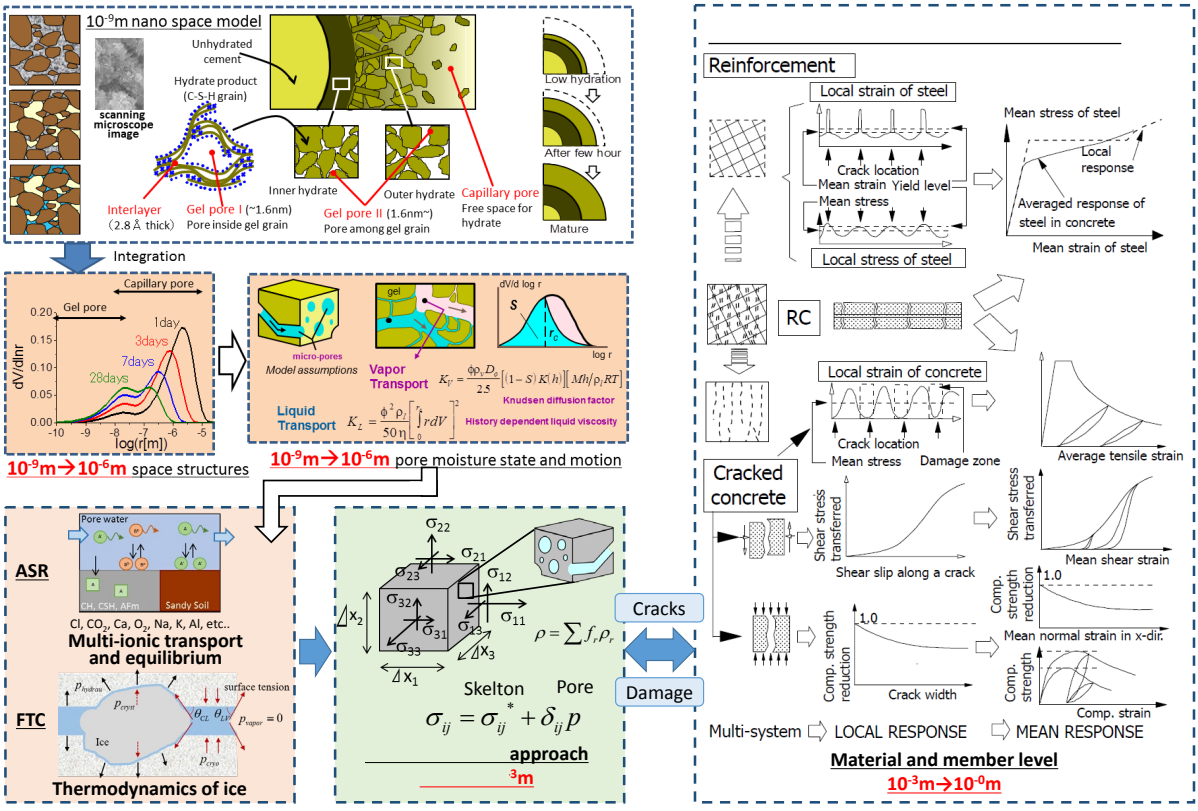

Fig. 1 Multi-scale simulation scheme of ASR and FTC induced deformation (Maekawa *et al.*, 2008)

The multi-scale integrated simulation scheme has been summarized in **Fig. 1**. Starting from the hydration stage at nano-scale, the chemical reactions are computationally reproduced based on the hydration kinetics (Maekawa *et al.*, 2008). Then, the hydration products together with the cement particles forms the micro pore structure, within which the moisture transport and equilibrium can be formulated. The multi-ionic transport and

equilibrium for ASR, as well as the thermodynamic equilibrium of ice formation are also considered at this scale (Takahashi *et al.*, 2016, Scherer and Valenza II, 2005). Since both ASR and ice formation will cause volume increase in the pore substances, mechanical interactions between pore substances (ice, water, ASR gel) and concrete skeleton shall be considered for both non-cracked and cracked conditions. During the poro-mechanical modeling, the liquid water movement and ASR gel migration are also calculated according to their pressure gradients. As the pore pressure by ASR is a long-time sustained force and the FTC will cause daily cyclic loads to solid skeletons, the time-dependent and cyclic nonlinearity should be adopted (Maekawa *et al.*, 2006).

2.1 Micro-mesoscale Coupling Model

The coupled FTC and ASR effect will be investigated from the micro pore structure level, and up-scaled to the meso-scale level by means of space-averaging integral. **Figure 2** illustrates the representative volume element (RVE) for this two-scale problem. Considering a RVE at meso-scale (1mm to 1cm) which contains aggregate, cement paste, entrained air and meso-cracks, the ASR gel will be created in and around aggregates, while the ice will develop in meso-cracks (if the cracks are filled by free water). The semi-liquid ASR gel can flow into the meso-cracks and entrained air voids through the micro-pore system (Jensen *et al.*, 1984, Maraghechi *et al.*, 2012), the ASR gel in meso-cracks can reduce the water transport and ice formation, which is beneficial to frost resistance of composite. However, if the entrained air bubbles are filled by the ASR gel, they may also lose their function in preventing the frost damage.

At the micro pore structure level (10μm to 100μm), the ice grows first from the larger capillary pores. But, if the greater capillary pores would be already occupied by ASR gel, the ice formation will be delayed with less amount, and finally result in a smaller frost expansion. The amount of intruded ASR gel in capillary pores also relies on the tensile capacity of concrete matrix, which can be affected by the damage level and the confining conditions (like steel reinforcement). The aforementioned events are very sensitive to the surface tension of ASR gel, for which more experimental investigations are necessary.

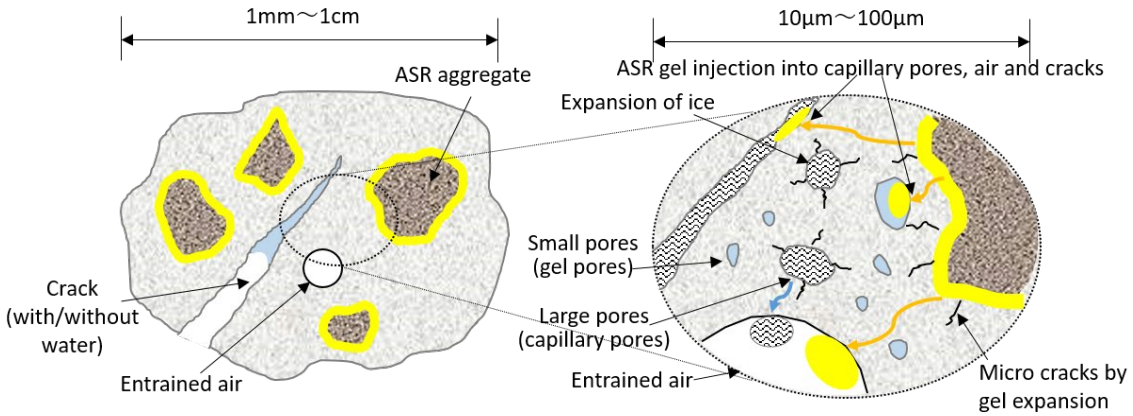

Fig. 2 Micro-meso-scale coupled ASR expansion and ice formation (Gong *et al.*, 2017)

The coupling problem at microscale closely relies on the pore size distribution, which can be described by a simple Raleigh-Ritz (R-R) distribution function as follows (Maekawa *et al.*, 2008):

$$\phi(r) = \phi_{lr} + \phi_{gel}\left(1-\exp(-B_{gel}r)\right) + \phi_{cap}\left(1-\exp(-B_{cap}r)\right) \quad (1)$$

where $\phi(r)$ is the cumulated porosity whose radii are less than r, ϕ_{lr}, ϕ_{gel} and ϕ_{cap} are the porosity of interlayer, gel and capillary pores, respectively, B_{gel} and B_{cap} are the solo porosity distribution parameter for the gel and capillary pores. The critical radius (r_{ASR}) of the pore into which ASR gel can intrude under a gel pressure (p_{ASR}) can be determined as:

$$r_{ASR} = \frac{2Z_{ASR}}{p_{ASR}} \tag{2}$$

where $Z_{ASR} = \gamma_{ASR} \cos\theta_{ASR}$, γ_{ASR} is the specific energy of ASR gel and θ_{ASR} is the contact angle between ASR gel and concrete skeleton. The parameter $Z_{ASR} \approx 0.4$ is determined based on the sensitivity analysis using the free expansion data from Muranaka and Tanaka (2013). Similarly, the ice occupation of different sizes of pores depends on the thermodynamic equilibrium (Scherer and Valenza II, 2005):

$$r_{ICE} = \frac{2Z_{ICE}}{\Delta S_{fv} \cdot (T_0 - T)} + \delta \tag{3}$$

where $Z_{ICE} = \gamma_{ICE} \cos\theta_{ICE}$, $\gamma_{ICE} \approx 0.04$ J/m^2 is the specific energy of ice/water interface, $\theta_{ICE} \approx 0$ is the contact angle between ice and pore wall, $\Delta S_{fv} \approx 1.2$ J/(cm^3·K) is the molar entropy of fusion, T<0°C is the local temperature in Celsius, T_0 is the freezing point of free water (0°C), $\delta \approx 0.9$ nm is the thickness of unfrozen water layer between ice and pore wall.

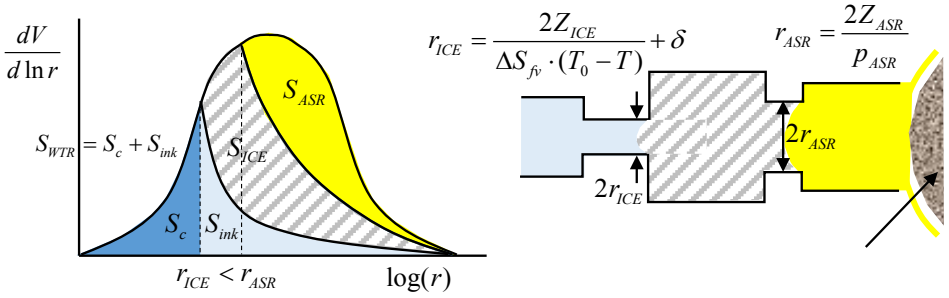

Fig. 3 ASR gel intrusion and ice formation in pores considering the pore size and shape (Gong *et al.*, 2017)

It is obvious that when ASR takes place first, the ice will not start to form until $r_{ICE} < r_{ASR}$, as shown in **Fig. 3**. The so-called "ink-bottle" effect needs to be considered for both ice formation and ASR gel intrusion, which is caused by the differences in size between pore entry and pore body (see **Fig. 3**). This part of the pore volume can be evaluated as (Maekawa *et al.* 2008):

$$S_{ink} = \int_{\min(r_{ICE}, r_{ASR})}^{\infty} f_r \Omega dr = \int_{\min(r_{ICE}, r_{ASR})}^{\infty} \left(\frac{S_c}{V}\right) dV = -S_c \ln(S_c) \tag{4}$$

where S_{ink} is the ratio of the trapped water to the total pore space, Ω is the normalized pore size distribution ($\int_0^\infty \Omega dr = 1$), $S_c = \int_0^{\min(r_{ICE}, r_{ASR})} \Omega dr$ is the equilibrium water content even when no water is trapped, $f_r = S_c/V$ is the probability that the water can be trapped by the ink bottle effect. It is obvious that S_{ink} will depend on the minimum value of r_{ICE} and r_{ASR} (**Fig. 3**).

Other than the micro-pores, the entrained air bubbles are also important to the frost damage and ASR expansion. The air bubbles can hold the expanded ASR gel, but at the same time, the filled bubbles will stop function to prevent the frost damage. A simplistic rate-dependent model of ASR gel flow is assumed as:

$$\dot{V}_{ASR \to AIR} = k_{AIR} \cdot (1 - \beta_{ASR \to AIR}) \cdot p_{ASR} \cdot Air \tag{5}$$

where $\dot{V}_{ASR \to AIR}$ is the speed of gel flow into air bubbles, k_{AIR} is a constant which can be determined by the sensitivity analysis (3×10^{-9}Pa^{-1}s^{-1}), $\beta_{ASR \to AIR} = V_{ASR \to AIR} / Air$ is the ASR gel occupying ratio in the air bubbles (0 to 1), Air is the total air content (entrained and entrapped air). The functional air bubbles for the frost resistance is around 10% of the total air volume (Gong *et al.*, 2017, Promentilla and Sugiyama, 2010). Thus, if the ASR gel occupation ratio is larger than 10%, the frost resistance from entrained air will totally disappear.

Finally, the effective volume of ASR gel (ΔV_{ASR}) and ice expansion (ΔV_{ICE}) which can contribute to the poro-mechanical expansion are:

$$\Delta V_{ASR} = V_{ASR\_TOTAL} - S_{ASR} - V_{ASR\rightarrow AIR} \tag{6}$$

$$\Delta V_{ICE} = 0.09 S_{ICE} - \max(0.1 Air - V_{ASR\rightarrow AIR}, 0) \tag{7}$$

where the total created ASR gel volume (V_{ASR_TOTAL}) is formulated as a function of the alkali concentration, updated free water and the content of reactive aggregates. The environmental variable such as the temperature and relative humidity have also been considered to affect the gel generation rate (Takahashi *et al.*, 2016).

2.2 Poromechanical Modeling of Mixed Pore Substances

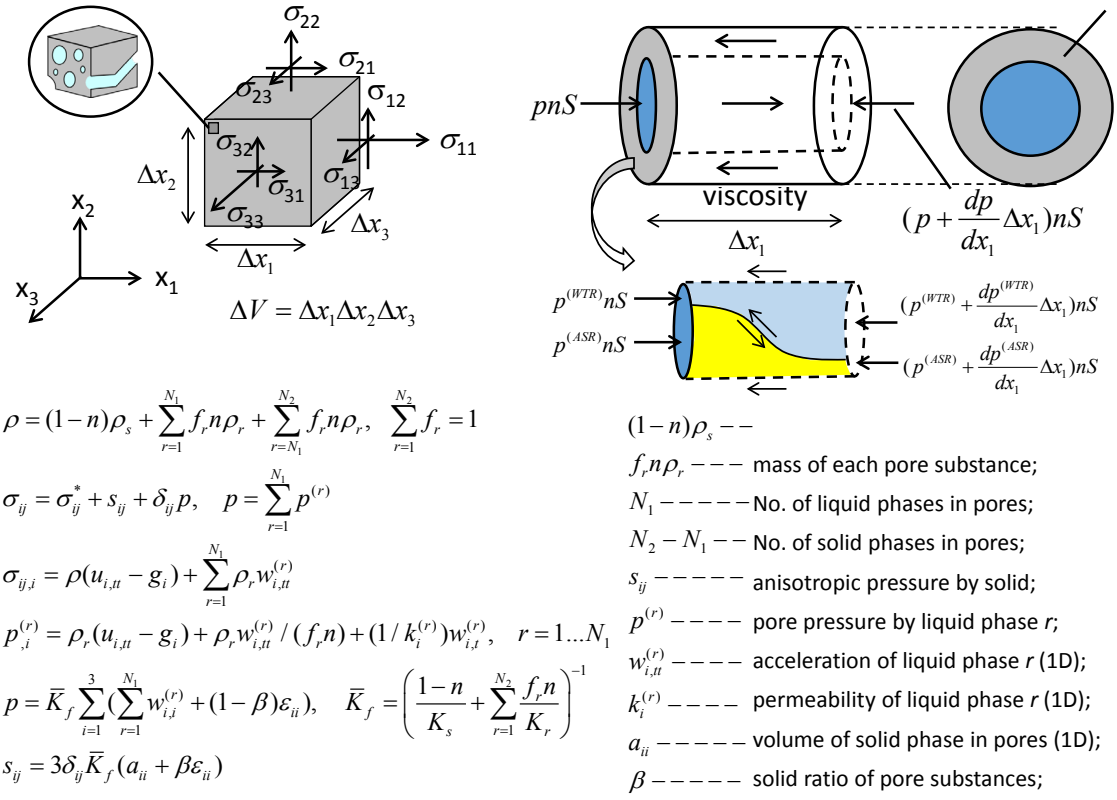

$$\rho = (1-n)\rho_s + \sum_{r=1}^{N_1} f_r n \rho_r + \sum_{r=N_1}^{N_2} f_r n \rho_r, \quad \sum_{r=1}^{N_2} f_r = 1$$

$$\sigma_{ij} = \sigma_{ij}^{*} + s_{ij} + \delta_{ij} p, \quad p = \sum_{r=1}^{N_1} p^{(r)}$$

$$\sigma_{ij,i} = \rho(u_{i,tt} - g_i) + \sum_{r=1}^{N_1} \rho_r w_{i,tt}^{(r)}$$

$$p_{,i}^{(r)} = \rho_r (u_{i,tt} - g_i) + \rho_r w_{i,tt}^{(r)} / (f_r n) + (1/k_i^{(r)}) w_{i,t}^{(r)}, \quad r = 1 \ldots N_1$$

$$p = \bar{K}_f \sum_{i=1}^{3} (\sum_{r=1}^{N_1} w_{i,i}^{(r)} + (1-\beta)\varepsilon_{ii}), \quad \bar{K}_f = \left(\frac{1-n}{K_s} + \sum_{r=1}^{N_2} \frac{f_r n}{K_r} \right)^{-1}$$

$$s_{ij} = 3\delta_{ij} \bar{K}_f (a_{ii} + \beta \varepsilon_{ii})$$

$(1-n)\rho_s$ – –

$f_r n \rho_r$ – – – mass of each pore substance;

N_1 – – – – – No. of liquid phases in pores;

$N_2 - N_1$ – – No. of solid phases in pores;

s_{ij} – – – – – anisotropic pressure by solid;

$p^{(r)}$ – – – – pore pressure by liquid phase *r*;

$w_{i,tt}^{(r)}$ – – – – acceleration of liquid phase *r* (1D);

$k_i^{(r)}$ – – – – permeability of liquid phase *r* (1D);

a_{ii} – – – – – volume of solid phase in pores (1D);

β – – – – – solid ratio of pore substances;

Fig. 4 Poro-mechanical approach for skeleton deformation and local strong-coupled multi-phase flow (Biot, 1963, Maekawa *et al.*, 2013, Gong *et al.*, 2017)

The overall framework of the multi-phase poro-mechanical modeling is summarized in **Fig. 4**. Based on the two-phase model in previous studies (Maekawa *et al.*, 2008, Biot, 1963), the governing equations are extended to the multi-phase case. First, the averaged density (ρ) of the whole material becomes:

$$\rho = (1-n)\rho_s + \sum_{r=1}^{N_1} f_r n \rho_r + \sum_{r=N_1}^{N_2} f_r n \rho_r \tag{8}$$

where 1-n and ρ_s are the volume ratio and density of concrete skeleton, f_r is the proportion of each solid/liquid substance in pores and $\sum_{r=1}^{N_2} f_r = 1$, N_2 is the total number of pore substances, N_1 is the number of liquid phase in pores, ρ_r is the density of each pore substance.

The movement of each pore liquid denoted by $U_i^{(r)}$ is expressed by the space-averaged displacement of concrete skeleton u_i and the substantial relative displacement of each pore liquid phase ($w_i^{(r)}$) as,

$$U_i^{(r)} = u_i + \frac{w_i^{(r)}}{f_r n} \tag{9}$$

The total stress (σ_{ij}) is composed of effective stress on the concrete skeleton (σ_{ij}^*), the stress caused by solid pore substances (s_{ij}), and the isotropic pore pressure (p):

$$\sigma_{ij} = \sigma_{ij}^* + s_{ij} + \delta_{ij} p \tag{10}$$

where δ_{ij} means the Kronecker's delta ($\delta_{ij} = 0$ if $i \neq j$; $\delta_{ij} = 1$ if $i = j$). The total pore pressure p is a sum of all the partial pressures of each liquid phase:

$$p = \sum_{r=1}^{N_1} p^{(r)} \tag{11}$$

The dynamic equilibrium equations of the concrete skeleton and each pore liquid in cracks can be formulated as follows:

$$\sigma_{ij,j} = \rho(u_{i,tt} - g_i) + \sum_{r=1}^{N_1} \rho_r w_{i,tt}^{(r)} \tag{12}$$

$$p_{,i}^{(r)} = \rho_r (u_{i,tt} - g_i) + \rho_r w_{i,tt}^{(r)} / (f_r n) + (1/k_i^{(r)}) w_{i,t}^{(r)}, \quad r = 1 \ldots N_1 \tag{13}$$

where g_i is the gravity and the last term of Eq. (13) represents the dragging action of each pore liquid based on Darcy's law, $k_i^{(r)}$ is the permeability of pore liquid r in each i-direction through concrete pore and crack gaps. The subscript t and tt denotes the first and second-degree differentiations with respect to time.

The total liquid and solid pore pressure in pores and crack system can be calculated as an extension of previous models (Biot, 1941, Biot, 1963, Maekawa *et al.*, 2008, Gebreyouhannes and Maekawa, 2016) as follows.

$$p = \overline{K}_f \sum_{i=1}^{3} \left(\sum_{r=1}^{N_1} w_{i,i}^{(r)} + (1-\beta)\varepsilon_{ii} \right) \tag{14}$$

$$s_{ij} = 3\delta_{ij} \overline{K}_f (a_{ii} + \beta \varepsilon_{ii}) \tag{15}$$

$$\overline{K}_f = \left(\frac{1-n}{K_s} + \sum_{r=1}^{N_2} \frac{f_r n}{K_r} \right)^{-1} \tag{16}$$

where $\overline{K}_f$ is the average bulk modulus of the whole composite assuming a volumetric linearity, ε_{ii} is the strain of concrete skeleton based on the space averaged path and time dependent constitutive equation rooted in the multi-directional crack modeling (Maekawa and Fujiyama, 2013, Maekawa *et al.*, 2003), a_{ii} is the amount of all generated solid pore substances, β is the ratio of the solid phase of pore substances. Thus, $\sum_{i=1}^{3} (\sum_{r=1}^{N_1} w_{i,i}^{(r)} + (1-\beta)\varepsilon_{ii})$ represents the volumetric strain of liquid phases inside concrete, while $a_{ii} + \beta\varepsilon_{ii}$ means the one-dimensional strain of solid pore substances.

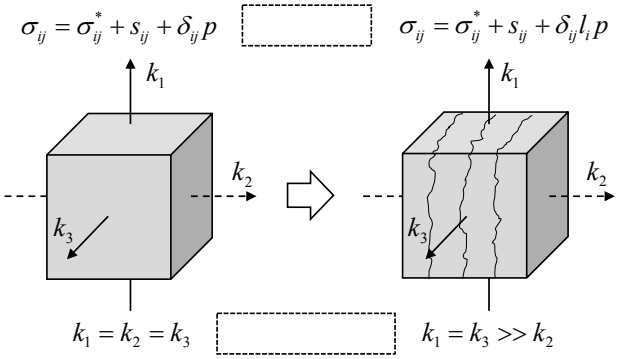

Fig. 5 Anisotropy of stress and permeability induced by cracking, considering the interactive effect of ASR gel and ice in cracks (Maekawa *et al.*, 2013)

The anisotropy of cracking can affect both liquid pore pressures and the liquid permeability, as discussed and formulated in Maekawa *et al.* (2013). Once the cracks are generated, the liquid pore substances (water, liquid ASR gel) are located within thin crack opening, and the interaction with cracked concrete is rather anisotropic. Therefore, the liquid pressure inside the crack gaps will act perpendicularly to a pair of parallel crack planes (**Fig. 5**) as,

$$\sigma_{ij} = \sigma^*_{ij} + s_{ij} + \delta_{ij} l_i p \tag{17}$$

where l_i is the unit directional vector normal to a crack plane. Here, the anisotropic liquid pore pressure will be considered only after complete formation of connected planes through the fracture process zones.

The crack opening will also result in an anisotropy in the permeation of pore liquids (**Fig. 5**). This anisotropy has been discussed for several pore liquids such as water (Maekawa *et al.*, 2013), steel corrosion gel (Gebreyouhannes and Maekawa, 2016) and the ASR gel (Takahashi *et al.*, 2016) as a single pore media. For a multi-directional cracking system, the permeability enlargement depends on the crack opening width of other two directions, which has been proposed as (Maekawa *et al.*, 2013),

$$k_i = k_0 \left\{ 1 + \left(\frac{\varepsilon_{jj} + \varepsilon_{kk}}{a} \right)^b \right\} \tag{18}$$

where k_i is the permeability in direction i, k_0 is the intrinsic permeability for different kinds of liquid, $\varepsilon_{jj}+\varepsilon_{kk}$ is the transverse in-plain strain of projection, a is a constant meaning the threshold of the crack opening (=100μ in this study), b is a constant related to the liquid type. Based on the experimental data from Wang *et al.* (1997), $k_0=10^{-9}$ cm/s, b=4 for liquid water, while for the liquid ASR gel, the sensitivity analysis (Takahashi *et al.*, 2016) based on measured ASR expansion shows $k_0=10^{-18}$ cm/s, b=2. When both ASR gel and liquid water are existed in cracks, the water motion will be retarded due to the partially filled crack path by ASR gel.

3. Simulations and Discussions

The FEM analysis is conducted by using DuCOM-COM3 for the coupled ASR and FTC expansion. Cubic concrete samples of 10cm are used in order to address the basic expansion, and the deformation is space-averaged similar to the experimental methods by using transducers or embedded sensors of "finite" sizes (see **Fig. 6**). In order to provide the same amount of generated ASR gel, the content of reactive aggregates is kept constant (1165kg/m^3 gravel and 777kg/m^3 sand) for all cases. Finally, the water to cement ratio (w/c) is set as 0.5 and the initial NaOH concentration is set as 1.64 mol/L.

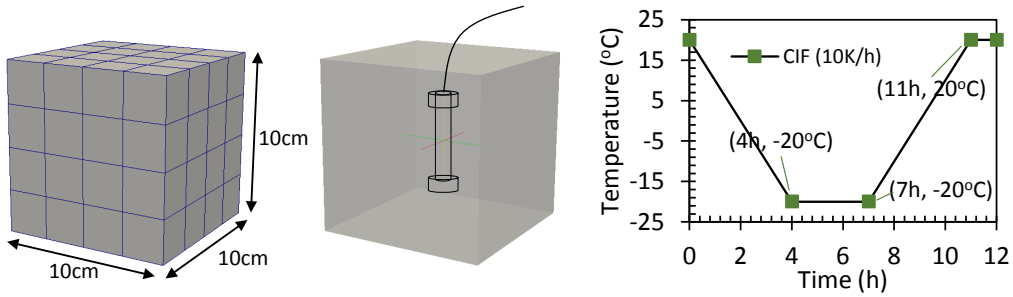

Fig. 6 FEM mesh and the equivalent embedded sensor

Table 1 Curing and exposure conditions of each group

	NaOH (mol/*l*)	Curing	Stage 1	Stage 2
ASR+FTC	1.64	28d, 20°C, 99.9%[1]	ASR: 137d, 40°C, 99.9%	FTC: 15d, $T(t)$[2], in water[3]
FTC+ASR	1.64	28d, 20°C, 99.9%	FTC: 15d, $T(t)$, in water	ASR: 137d, 40°C, 99.9%

[1]: In air, *RH*=99.9%, [2]: FTC temperature history, [3]: Continuous water supply during FTC

The curing and exposure conditions are listed in **Table 1**. After 28 days of curing (20°C, *RH*=99.9%), 137 days of ASR exposure and 15 days (30 cycles) of FTC are conducted with different sequences. The temperature history for each FTC follows **Fig. 6**.

3.1 Effect of ASR on FTC deformation

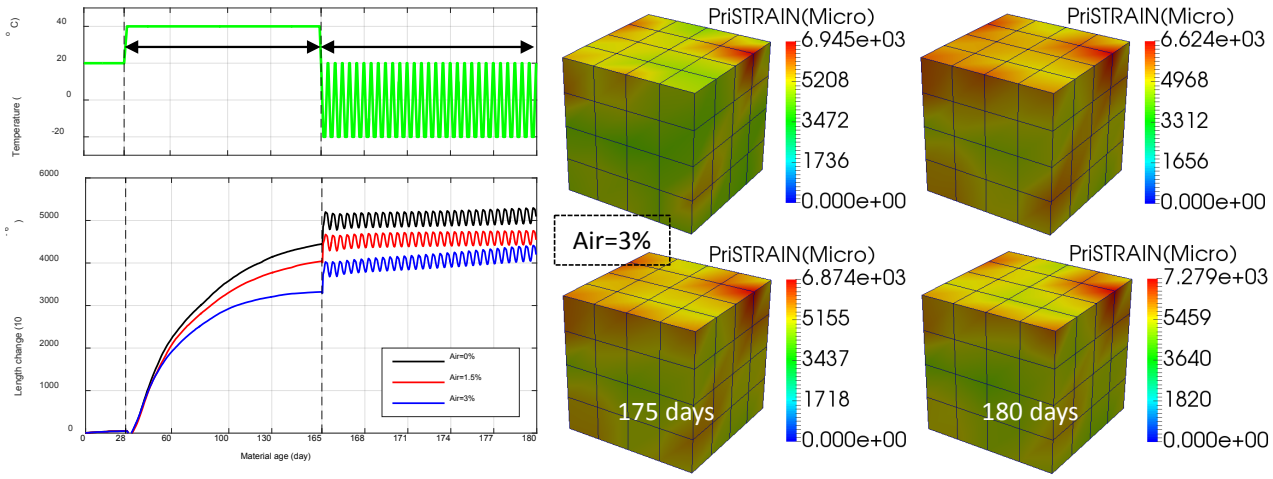

Fig. 7 Strain history and non-uniform damage of couple ASR (1st stage) and FTC (2nd stage)

The first discussion is on how the ASR will affect FTC expansion, that is, after curing stage, conducting ASR exposure for 137 days at 40°C and then followed by 30 cycles (20°C to -20°C) of freeze-thaw expansion. The deformation histories with different amount of entrained air are shown in **Fig. 7**, as well as the principle strain for the case of *Air*=3%. The ASR expansion can be reduced as more air is entrained, which is consistent with the experimental phenomena (Jensen *et al.*, 1984). After ASR exposure, only a slight increment in the deformation can be seen during the 30 FTCs, because of the reduced water uptake in the ASR gel filled cracks. The expansion is not perfectly uniform, but showed the random localization. This is natural and mainly due to the randomness on multi-directional crack's opening under a rather uniform field of stresses before cracking

and the broken symmetry is simply reproduced by using parallel computing process (Gebreyouhannes and Maekawa, 2016).

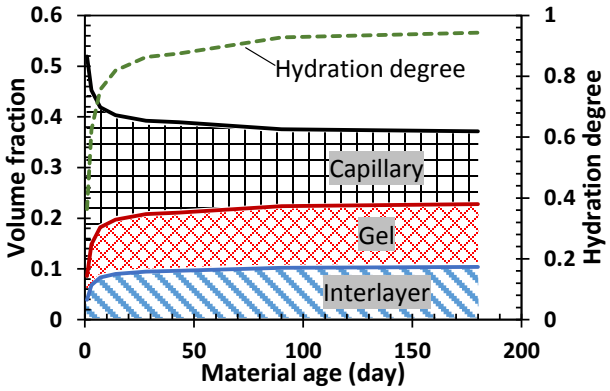

Fig. 8 Micro-porosity of cement paste during hydration

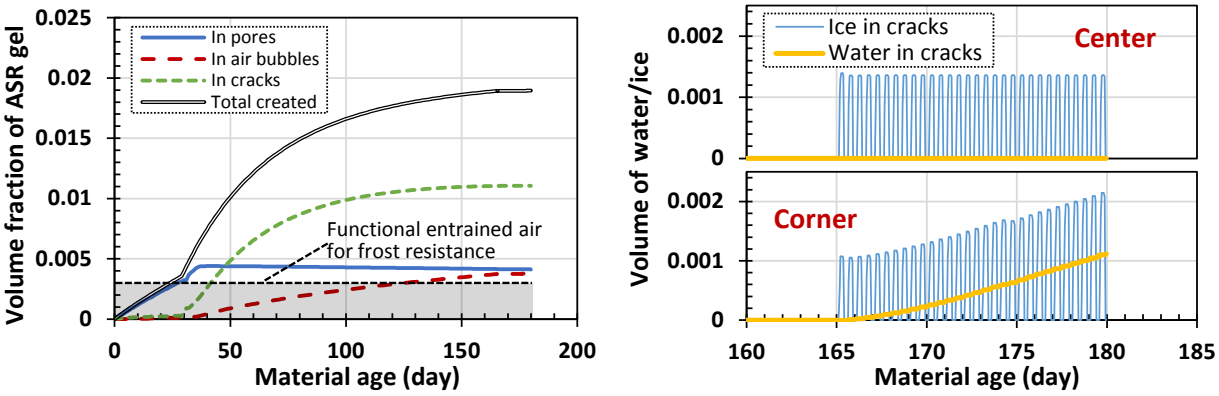

Fig. 9 Micro-chemo-physical events of ASR gel, water and ice (ASR+FTC, *Air*=3%)

The mechanisms behind the deformational behaviors in **Fig. 7** can be revealed through the micro-chemo-physical events. The hydration process can be calculated based on the kinetics model installed in DuCOM (Kishi and Maekawa, 1995), and the volume fraction of each kind of pores in cement paste (*w/c*=0.5) can be seen in **Fig. 8**. The pore space takes a considerable proportion in the cement paste (around 40%), and even for concrete (paste ratio around 25%), the total void ratio possibly gets 10%. Therefore, the pore space has a big capacity for the created ASR gel if the accessibility is guaranteed. **Fig. 9** shows the locations of ASR gel and moisture. Giving the total created ASR gel about 2% of total concrete volume, only a small part can be intruded into the capillary pores and entrained air (0.5% for each) based on the current parameters. The rest of it is the ASR gel in cracks, which will contribute to the expansion of concrete skeleton. During the FTC stage, only the moisture at the corner of concrete cube increases slightly (0.1%), while the center keeps constant (**Fig. 9**). This is because the crack space is almost fully occupied by ASR gel and the surrounding liquid water cannot penetrate inside.

In case where the total entrained air is 3%, the effective amount for frost resistance is around 0.3%. Then, the ASR gel has already occupied those air bubbles after the 165 days of exposure (see **Fig. 9**). As a result, even for the air-entrained concrete, the FTC expansion will still take place. This phenomenon is in harmony with the experiments of Bérubé *et al.* (2002), see **Fig. 10**. With air content of 6.4% and 2.4%, concrete is not likely to expand under FTC. However, after the ASR exposure, air bubbles will lose their functions in preventing the FTC expansion. Although it is difficult to quantify the exact experimental conditions in Bérubé *et al.* (2002), the experimental phenomena can still prove the findings of this study.

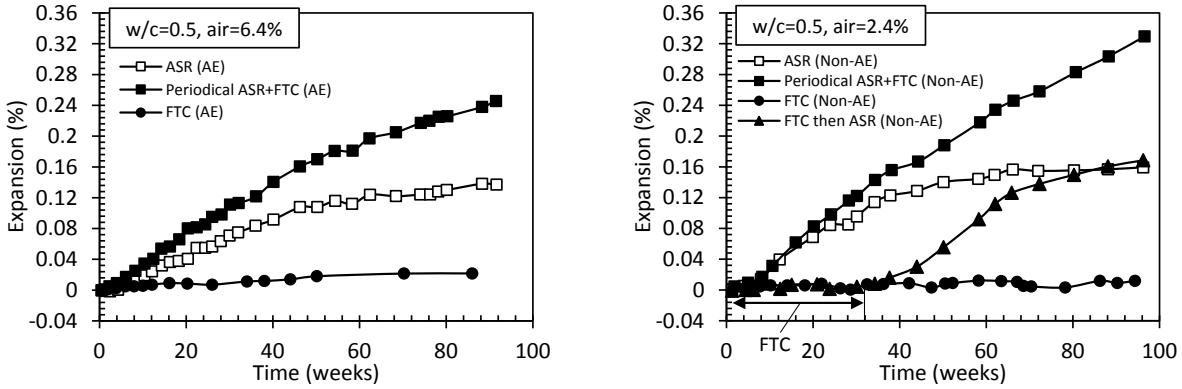

(a) (b)

Fig. 10 Experimental data of AE and non-AE concrete under combined periodical ASR and FTC (a) AE concrete (b) non-AE concrete (redraw from Bérubé *et al.* (2002))

3.2 Effect of FTC on ASR deformation

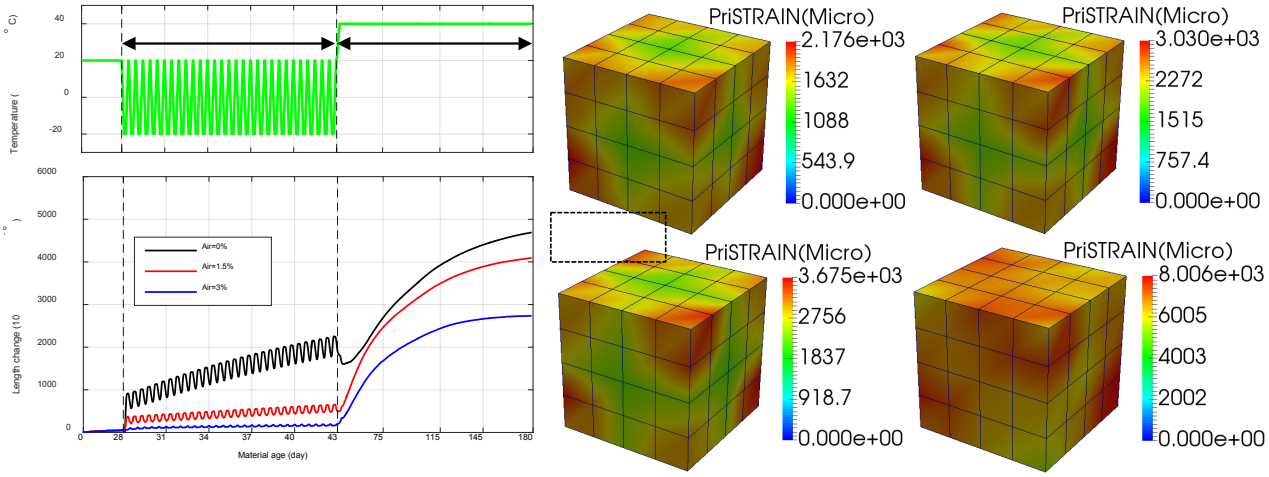

Fig. 11 Strain history and non-uniform damage of couple FTC (1st stage) and ASR (2nd stage)

The cases that FTC goes first followed by ASR are simulated as well. **Figure 11** shows the full strain history of concrete with different air volume, together with the principle strain distribution of the case *Air*=0%. The FTC expansion is highly depending on the air content, and 3% entrained air can totally terminate frost damage. The case of 0% has the biggest expansion, and deformational profile is closely related to the accessibility of heat and moisture, that is to say, the damage is most serious at the corners while the inner part is less. On the contrary, the later ASR expansion is rather uniform within the concrete cube, and non-uniformity in damage can be reduced finally.

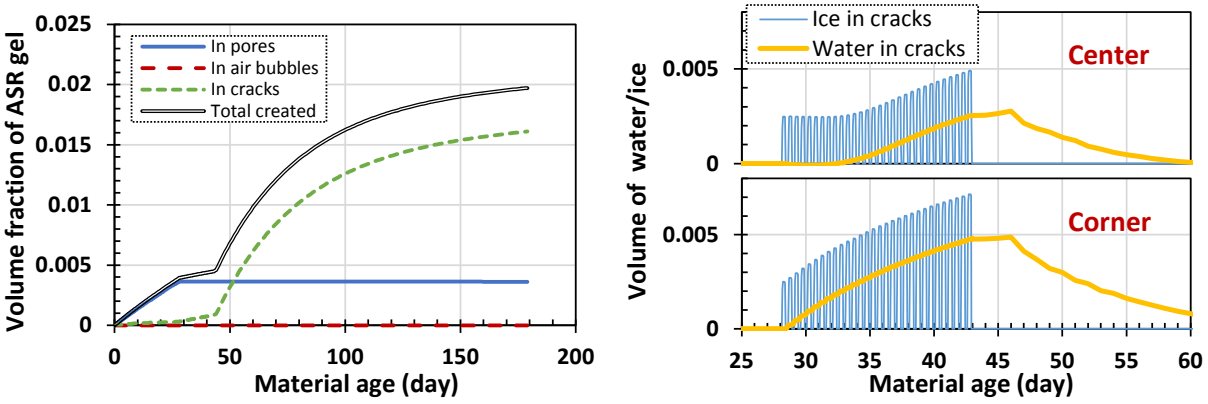

Fig. 12 Micro-chemo-physical events of ASR gel, water and ice (FTC+ASR, *Air*=0%)

For the case of *Air*=0%, the created ASR gel can only stay in pores or cracks, as shown in **Fig. 12**. It can also be seen that during the FTC stage (28days to 43 days), the created ASR gel is mainly absorbed by capillary pores, while little gel remains in cracks. Therefore, the water motion in between crack planes will not be affected by ASR gel. Consequently, both the corner and center part have a larger water uptake compared to **Fig. 9**. Finally, as the ASR exposure starts, the crack space will gradually be occupied by ASR gel, and the moisture in cracks will finally decrease to zero.

3.3 Residual mechanical responses

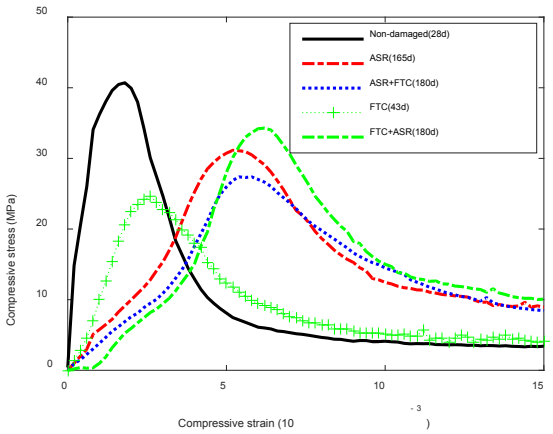

Fig. 13 The residual compressive behaviors after different exposure conditions

The coupled effect on the strength change and the stress-strain curves are shown in **Fig. 13**. The frost damage will no doubt result in a degradation in the mechanical responses, while the ASR gel can reduce this damaging effect, because the semi-liquid ASR gel in cracking system can bear compressive forces, enhance the tension-softening and shear capacity of crack gaps. For the coupled damage, when ASR takes place first, the following FTC will cause new cracks which are not filled by ASR gel. Then, the stiffness and strength will be slightly reduced. On the contrary, when FTC damage occurs first, the following ASR can significantly strengthen the pre-damaged concrete, even though the expansion becomes larger, because all the cracks gaps may be filled by ASR gel.

3.4 Size effect on the coupling damage

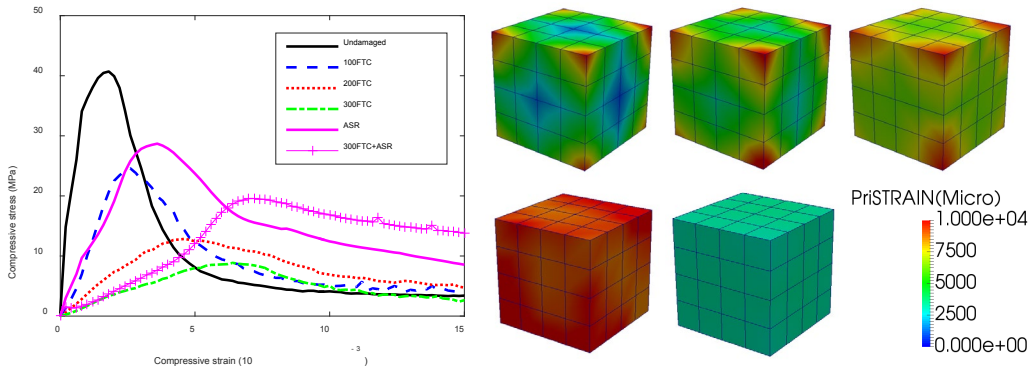

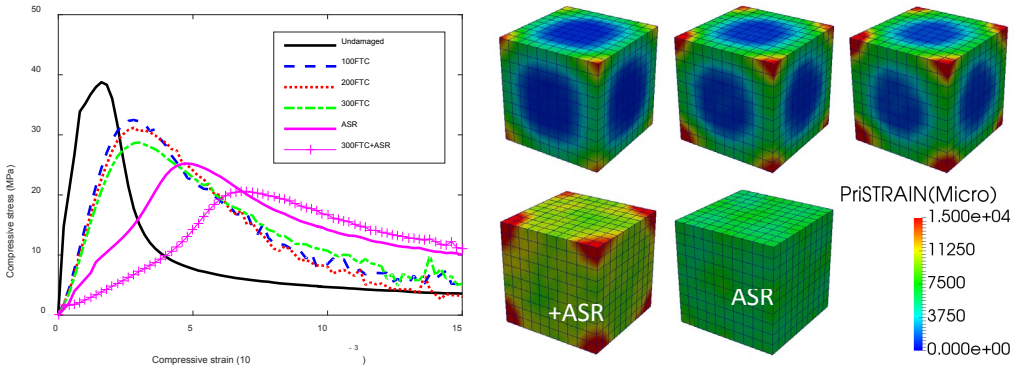

Fig. 14 Size effect on the coupled deformation and residual compressive behaviors

The complex coupled damages to the compressive strength of concrete cubes with different sizes are shown in **Fig. 14**. The gradually degraded compressive behavior during FTC agrees well with experimental observations (Duan *et al.*, 2011). The frost damage level becomes considerably large within the whole specimen of smaller size, but keeps limited values in the core part of larger ones due to the delayed heat and moisture transfer. As a result, when the number of FTC increases from 100 to 300, the smaller concrete shows significant reduction in strength while the larger one shows little difference. If the ASR exposure is followed by 300 FTC, the ASR gel may strengthen the serious frost damaged concrete (10cm cube), but it may also reduce the strength if the frost damage level is small (40cm cube), depending on which damaging effect is greater (ASR or FTC). Finally, the coupled damage is always greater than the single event of ASR, for both smaller and larger specimens. In sum, the size of concrete is more sensitive for the frost damage than the ASR damage.

4. Conclusions

Expansive damages caused by combined ASR and FTC are modeled through a poro-mechanical approach, by considering the strongly coupled physical events of the gel intrusion and ice formation in pores, gel movement and unfrozen water suction into entrained air, as well as the gel and water migration through damage cracks. Furthermore, based on the meso-scale nonlinear mechanics of concrete materials with cracks, deformation and cracking under mutually coupled effects are simulated in accordance with several sequences of combination.

The FEM simulation results show that the ASR gel may fill the air system and disable its function for the frost resistance. But at the same time, the water permeation in the crack system can also be retarded if the ASR gel occupies a big proportion of crack space. From the deformation profile, the ASR expansion is rather uniform only with some small localization caused by the broken symmetry. On the contrary, the frost damage is closely relying on the accessibility of heat and moisture, that is, the boundary area can be seriously damaged while the inner part is less affected. Finally damage uniformity of the coupling problem will lay between those in single ASR and single FTC.

Mechanically speaking, ASR and FTC expansion have different impacts on the residual compressive strength, because the ASR gel in the crack gaps may strengthen the damaged skeleton solids of concrete by solidification with calcium ion in pore solution. We have two chemo-physics events which produce damaging by FTC and ASR accompanying volume expansion inside porous media. At the same time, the authors focus on the remedy action of ASR gel in cracks to strengthen the damaged skeleton as a filler. Thus, the final apparent strength is clarified to depend on the sum of those three impacts with positive and negative aspects on the macroscopic figure.

The authors present behavioral simulations on the combined ASR and FTC events of concrete composites. Some of the findings are verified with previous experiments in this study, and someone remains un-proved and scientifically unknown. More detailed experimental verification is also required, which will be quantitatively conducted in future.

Acknowledgements

This study was financially supported by Council for Science, Technology and Innovation, "Cross-ministerial Strategic Innovation Promotion Program (SIP), Infrastructure Maintenance, Renovation and Management" granted by Japan Science and Technology Agency.

References

Bérubé, M.-A., Chouinard, D., Pigeon, M., Frenette, J., Boisvert, L. and Rivest, M. (2002), "Effectiveness of sealers in counteracting alkali-silica reaction in plain and air-entrained laboratory concretes exposed to wetting and drying, freezing and thawing, and salt water", *Canadian Journal of Civil Engineering,* Vol. 29 No. 2, pp. 289-300.

Bangert, F., Kuhl, D. and Meschke, G. (2004), "Chemo‐hygro‐mechanical modelling and numerical simulation of concrete deterioration caused by alkali‐silica reaction", *International Journal for Numerical and Analytical Methods in Geomechanics,* Vol. 28 No. 7‐8, pp. 689-714.

Bažant, Z.P. and Steffens, A. (2000), "Mathematical model for kinetics of alkali–silica reaction in concrete", *Cement and Concrete Research,* Vol. 30 No. 3, pp. 419-28.

Biot, M.A. (1941), "General theory of three‐dimensional consolidation", *Journal of applied physics,* Vol. 12 No. 2, pp. 155-64.

Biot, M.A. (1963), "Theory of stability and consolidation of a porous medium under initial stress", *Journal of Mathematics and Mechanics,* Vol. 12 No. 4, pp. 521-41.

Charpin, L. and Ehrlacher, A. (2014), "Microporomechanics study of anisotropy of ASR under loading", *Cement and Concrete Research,* Vol. 63 pp. 143-57.

Costa, U., Mangialardi, T. and Paolini, A.E. (2014), "Assessment of blended cements effectiveness against ASR by mortar and concrete expansion tests", *Journal of Advanced Concrete Technology,* Vol. 12 No. 8, pp. 266-78.

Duan, A., Jin, W. and Qian, J. (2011), "Effect of freeze–thaw cycles on the stress–strain curves of unconfined and confined concrete", *Materials and structures,* Vol. 44 No. 7, pp. 1309-24.

Gebreyouhannes, E. and Maekawa, K. (2016), "Nonlinear gel migration in cracked concrete and broken symmetry of corrosion profiles", *Journal of Advanced Concrete Technology,* Vol. 14 No. 6, pp. 271-86.

Gong, F., Sicat, E., Ueda, T. and Zhang, D. (2013), "Meso-scale Mechanical Model for Mortar Deformation under Freeze Thaw Cycles", *Journal of Advanced Concrete Technology,* Vol. 11 No. 2, pp. 49-60.

Gong, F., Takahashi, Y. and Maekawa, K. (2017), "Strong coupling of freeze-thaw cycles and alkali silica reaction-Multi-scale poro-mechanical approach to concrete damages", *Journal of Advanced Concrete Technology,* Vol. 15 No. 7, pp. 346-67.

Hasan, M., Okuyama, H., Sato, Y. and Ueda, T. (2004), "Stress-strain model of concrete damaged by freezing and thawing cycles", *Journal of Advanced Concrete Technology,* Vol. 2 No. 1, pp. 89-99.

Jensen, A.D., Chatterji, S., Christensen, P. and Thaulow, N. (1984), "Studies of alkali-silica reaction—part II effect of air-entrainment on expansion", *Cement and Concrete Research,* Vol. 14 No. 3, pp. 311-4.

Kawabata, Y. and Yamada, K. (2015), "Evaluation of alkalinity of pore solution based on the phase composition of cement hydrates with supplementary cementitious materials and its relation to suppressing ASR expansion", *Journal of Advanced Concrete Technology,* Vol. 13 No. 11, pp. 538-53.

Kawamura, M., Takeuchi, K. and Sugiyama, A. (1994), "Mechanisms of expansion of mortars containing reactive aggregate in NaCl solution", *Cement and Concrete Research,* Vol. 24 No. 4, pp. 621-32.

Kishi, T. and Maekawa, K. (1995), "Multi-component model for hydration heat of portland cement", *Journal of JSCE,* Vol. No.526/V-29 pp. 97-109.

Maekawa, K. and Fujiyama, C. (2013), "Rate-dependent model of structural concrete incorporating kinematics of ambient water subjected to high-cycle loads", *Engineering Computations,* Vol. 30 No. 6, pp. 825-41.

Maekawa, K., Ishida, T., Chijiwa, N. and Fujiyama, C. (2013), "Multiscale coupled-hygromechanistic approach to the life-cycle performance assessment of structural concrete", *Journal of Materials in Civil Engineering,* Vol. 27 No. 2, p. A4014003.

Maekawa, K., Ishida, T. and Kishi, T. (2003), "Multi-scale modeling of concrete performance", *Journal of Advanced Concrete Technology,* Vol. 1 No. 2, pp. 91-126.

Maekawa, K., Ishida, T. and Kishi, T. (2008), *Multi-scale modeling of structural concrete,* CRC Press.

Maekawa, K., Soltani, M., Ishida, T. and Itoyama, Y. (2006), "Time-dependent space-averaged constitutive modeling of cracked reinforced concrete subjected to shrinkage and sustained loads", *Journal of Advanced Concrete Technology,* Vol. 4 No. 1, pp. 193-207.

Maraghechi, H., Fischer, G. and Rajabipour, F. (2012), "The role of residual cracks on alkali silica reactivity of recycled glass aggregates", *Cement and Concrete Composites,* Vol. 34 No. 1, pp. 41-7.

Multon, S., Sellier, A. and Cyr, M. (2009), "Chemo–mechanical modeling for prediction of alkali silica reaction (ASR) expansion", *Cement and Concrete Research,* Vol. 39 No. 6, pp. 490-500.

Muranaka, M. and Tanaka, Y. (2013), "Development of Physical and Chemical Model for Concrete Expansion due to Asr Based on Reaction Mechanism", *Journal of Japan Society of Civil Engineers, Ser. E2 (Materials and Concrete Structures),* Vol. 69 pp. 1-15.

Promentilla, M.A.B. and Sugiyama, T. (2010), "X-ray microtomography of mortars exposed to freezing-thawing action", *Journal of Advanced Concrete Technology,* Vol. 8 No. 2, pp. 97-111.

Saouma, V. (2014), *Numerical modeling of AAR,* CRC press.

Saouma, V.E., Martin, R.A., Hariri-Ardebili, M.A. and Katayama, T. (2015), "A mathematical model for the kinetics of the alkali–silica chemical reaction", *Cement and Concrete Research,* Vol. 68 pp. 184-95.

Scherer, G.W. and Valenza II, J.J. (2005), "Mechanisms of frost damage", in *Materials science of concrete,* American Ceramic Society, pp. 209-46.

Takahashi, Y., Ogawa, S., Tanaka, Y. and Maekawa, K. (2016), "Scale-dependent ASR expansion of concrete and its prediction coupled with silica gel generation and migration", *Journal of Advanced Concrete Technology,* Vol. 14 No. 8, pp. 444-63.

Wang, K., Jansen, D.C., Shah, S.P. and Karr, A.F. (1997), "Permeability study of cracked concrete", *Cement and Concrete Research,* Vol. 27 No. 3, pp. 381-93.